Title Oncogenic KRAS^{G12D} extrinsically induces an immunosuppressive microenvironment in lung adenocarcinoma

Short Title KRAS^{G12D} drives immunosuppression

Authors

Emily Lasse-Opsahl[1*], Rachael Baliira[1*], Ivana Barravecchia[2,3*], Elyse McLintock[2,3], Jennifer M. Lee[2,3], Sarah F. Ferris[2,3], Carlos E. Espinoza[4], Rachael Hinshaw[1], Sophia Cavanaugh[2], Marzia Robotti[2,3], Kristee Brown[4], Katelyn Donahue[1], Kristena Y. Abdelmalak[2,3], Craig J. Galban[2,5], Timothy L. Frankel,[4,6], Yaqing Zhang[4,6], Marina Pasca di Magliano[4,6,7], Stefanie Galban[2,3,4,6,**]**

*co-first authors

Affiliations
[1]Graduate Program in Cancer Biology, The University of Michigan Medical School, Ann Arbor, MI, 48109
[2]Deparment of Radiology, The University of Michigan Medical School, Ann Arbor, MI, 48109
[3]Center for Molecular Imaging, The University of Michigan Medical School, Ann Arbor, MI, 48109
[4]Department of Surgery, The University of Michigan Medical School, Ann Arbor, MI 48109
[5]Department of Biomedical Engineering, The University of Michigan Medical School and College of Engineering, Ann Arbor, MI 48109
[6]Rogel Cancer Center, The University of Michigan Medical School, Ann Arbor, MI 48109
[7]Department of Cell and Developmental Biology, The University of Michigan Medical School, Ann Arbor, MI 48109

****Corresponding Authors:**
Stefanie Galban, PhD
Center for Molecular Imaging
Department of Radiology
Department of Surgery
BSRB A502
The University of Michigan
Ann Arbor, MI 48109
(734) 764-4076

sgalban@umich.edu
Marina Pasca di Magliano
Department of Surgery
Department of Cell and Developmental Biology
Rogel Cancer Center Room 6306
1500 E. Medical Center Drive
The University of Michigan
Ann Arbor, MI 48109
marinapa@umich.edu

Conflict of Interest: no conflict of interest has been declared.

Note on authorship: the final author order is still fluid and might change based on data expected prior to peer reviewed publication.

ABSTRACT

Despite advancements in targeted and immunotherapies, lung cancer remains the leading cause of cancer-related deaths in both men and women worldwide. At 85%, non-small cell lung cancer (NSCLC) is by far the most common subtype, comprising adenocarcinomas, squamous cell carcinoma and large cell carcinoma. KRAS is commonly mutated in adenocarcinomas, with the most common point mutation being G12C (39%), followed by G12V (21%), G12D (17%), and G12A (10%). Notably, while $KRAS^{G12C}$ is the most prevalent mutation in adenocarcinoma among former or current smokers (42%), $KRAS^{G12D}$ is most common in patients who have never smoked (56%) [2]. Because nonsmokers have poorer prognosis, and mostly lack response to immunotherapy, we interrogated the immune changes in a previously described genetically engineered model of $Kras^{G12D}$ driven lung cancer. In this murine model, oncogenic Kras expression can be controlled genetically in the lung, allowing activation of oncogenic $Kras^{G12D}$ to initiate tumor growth, depletion of $Kras^{G12D}$ for tumor eradication, and re-activation of $Kras^{G12D}$ to model relapse. We demonstrate a $Kras^{G12D}$ dependent regulation of the tumor microenvironment depends on secreted factors derived from epithelial cells expressing oncogenic Kras, which regulates lung fibroblasts. Fibroblast derived secreted factors in turn drive an immune suppressive and tumor promoting phenotype in the lung, specifically through the polarization of macrophages. The identification of this oncogenic Kras-dependent secretome that supports lung tumor growth through crosstalk with the microenvironment provides new targets to develop alternative strategies for co-targeting KRAS mutant lung disease with Kras inhibitors or for treating recurring lung tumors.

Introduction

In 2021 over 235,000 new patients were diagnosed with lung cancer in the United States [3], 85% of those with non-small cell lung cancer (NSCLC). NSCLC is subclassified into three major groups: adenocarcinomas (40%), squamous cell carcinomas (30%), and large cell carcinomas (15%). KRAS is commonly mutated in adenocarcinomas, with the most common point mutation being G12C (39%), followed by G12V (21%), G12D (17%), and G12A (10%) [2]. Notably, while $KRAS^{G12C}$ is the most prevalent mutation in adenocarcinoma among former or current smokers (42%), $KRAS^{G12D}$ is most common in patients who have never smoked (56%) [2]. Nonsmokers have poorer prognosis, at least in part because they do not benefit from immunotherapy [4], possibly due to lower mutation burden—and thus, lower neoantigen prevalence.

While mutant KRAS was long deemed undruggable, several isoform specific inhibitors have recently entered the clinic. $KRAS^{G12C}$ inhibitors such as Sotorasib and Adagrasib have gained FDA approval for lung cancer, while MRTX1133, a $KRAS^{G12D}$ inhibitor, has now entered phase 1 clinical testing for different malignancies, including G12D-mutant lung cancer. While this is an exciting development, the prospect of resistance to targeted therapy is real; several examples of this have already been described for G12C inhibitors [5]. In at least some of these instances, resistance to Sotorasib has been linked to the remodeling of the tumor microenvironment [6, 7]. The effects of $Kras^{G12D}$ inactivation in lung adenocarcinoma, including changes in the tumor microenvironment and mechanisms of resistance, remain largely unknown.

Genetically engineered mouse models expressing oncogenic Kras upon Cre recombination, with or without mutation of the tumor suppressor p53, model the development of NSCLC resembling the human disease and are widely used for both basic discovery and preclinical studies [8]. A similar model, which allows both inducible and reversible expression of oncogenic

Kras^{G12D}, revealed that this oncogene is required not only for tumor initiation, but also for tumor maintenance, independently from the presence of additional mutations (such as inactivation/mutation of *Trp53* or other tumor suppressor genes) [9]. However, the effect of oncogenic Kras expression and subsequent inactivation in the tumor microenvironment in the lung has remained unexplored. Given the likely need to devise combination targeting modalities to prevent/overcome resistance to targeted Kras inhibitors, it is imperative to unravel the cellular crosstalk between Kras mutant epithelial cells and their surrounding microenvironment.

To study the extrinsic role of oncogenic Kras in lung cancer maintenance and progression, we modified a genetically engineered mouse model (GEMM) that expresses mutant Kras^{G12D} in an inducible and reversible manner in the lung epithelium. In the Lung-iKras model, first described by the Varmus laboratory [9], expression of oncogenic Kras in club cells, in combination with loss of function mutations in tumor suppressor genes, efficiently drives formation of lung adenocarcinoma in both male and female mice. Inactivation of oncogenic Kras^{G12D} in tumors results in tumor regression, establishing a role for oncogenic Kras^{G12D} in the maintenance of NSCLC.

We have re-derived the Lung-iKras model, incorporating the current understanding of lung cancer etiology [10-12]. While the initial model used a *Trp53* null allele of Ink4a null, we used an allele expressing mutant *Trp53*^{R172H} — as mutant alleles are more common than null in human cancer — in an inducible manner [13] wherein mutant Tp53 expression in the lung is activated by intranasal administration of adenovirus-Cre recombinase [9, 14]. Here, we used the Lung-iKras mouse to drive NSCLC in mouse lungs; we then inactivated oncogenic Kras and, as expected, observed tumor regression. Interestingly, characteristics of the microenvironment such as fibroblast activation status drastically changed upon Kras inactivation. To gather an unbiased

understanding of the effects of inactivating oncogenic Kras, we performed single cell RNA sequencing on lungs of iKras mice with $Kras^{G12D}$ ON or upon inactivation ($Kras^{G12D}$ OFF). In the presence of oncogenic Kras, macrophages in the lung expressed immunosuppressive markers, consistent with KrasG12D mutant tumors being poorly immunogenic. To understand how oncogenic Kras regulates the composition and differentiation status of macrophages, we used *ex vivo* approaches. Mechanistically, we show that fibroblasts are a key signaling hub, mediating interactions between epithelial cells and macrophages and thus potentially mediating the immune suppressive status of tumors.

Results

Inhibition of Kras^{G12D} results in tumor regression in L-iKras mouse model of lung adenocarcinoma. To generate a mouse model wherein oncogenic Kras can be induced and reversed in the lung with accompanying mutant Tp53 expression, the previously described bitransgenic mouse *CCSP-rtTa*; *TetO-Kras^{G12D}* [9] was crossed with the *Trp53$^{LSL-R172H}$* [9, 15] mouse. In this study, we will be referring to this genetically engineered mouse model (GEMM) as L-iKras (*CCSP-rtTa*; *TetO-Kras^{G12D}*; *Trp53$^{LSL-R172H/+}$*). Upon administration of doxycycline (dox) in the drinking water, expression of the reverse tetracycline transactivator (rtTa) can be induced in club cells of the lung, where it binds to the response element (*TetO-Kras^{G12D}*) to initiate lung specific expression of Kras^{G12D}. When dox is withdrawn from the drinking water, rtTA is inactivated in club cells and the expression of Kras^{G12D} is prevented/reversed. Conditional, lung specific expression of mutant Trp53^{R172H} in the lung can be achieved simultaneously by intranasal administration of adenovirus Cre-recombinase (ad-Cre) at study start (**Figure 1A**). Single transgenic mice given dox or triple transgenic mice that did not receive dox served as controls for this study. Controls also included single or triple transgenic mice given ad-Cre. Overall survival of the three experimental cohorts was compared to understand the impact on tumor growth of Kras^{G12D} expression alone or Kras^{G12D} with mutant Trp53 co-occurring mutation in the lung (**Figure 1B**). One experimental triple transgenic cohort was administered dox and ad-Cre to induce Kras^{G12D} and mutant Trp53 expression; a second group was given dox only to induce Kras^{G12D} expression but not mutant Trp53, while the control group, including mice that are single transgenic or mice with an activated *Trp53* mutant allele but lacking a *CCSP-rtTa* or *TetO-Kras^{G12D}* cassette, were given dox and ad-Cre for a period of 40 weeks. Mice expressing only Kras^{G12D} had a median survival of 38 weeks, though survival significantly declined after 30 weeks. Mice that expressed both Kras^{G12D} and Trp53 showed a median survival of only 20 weeks. Although the difference was

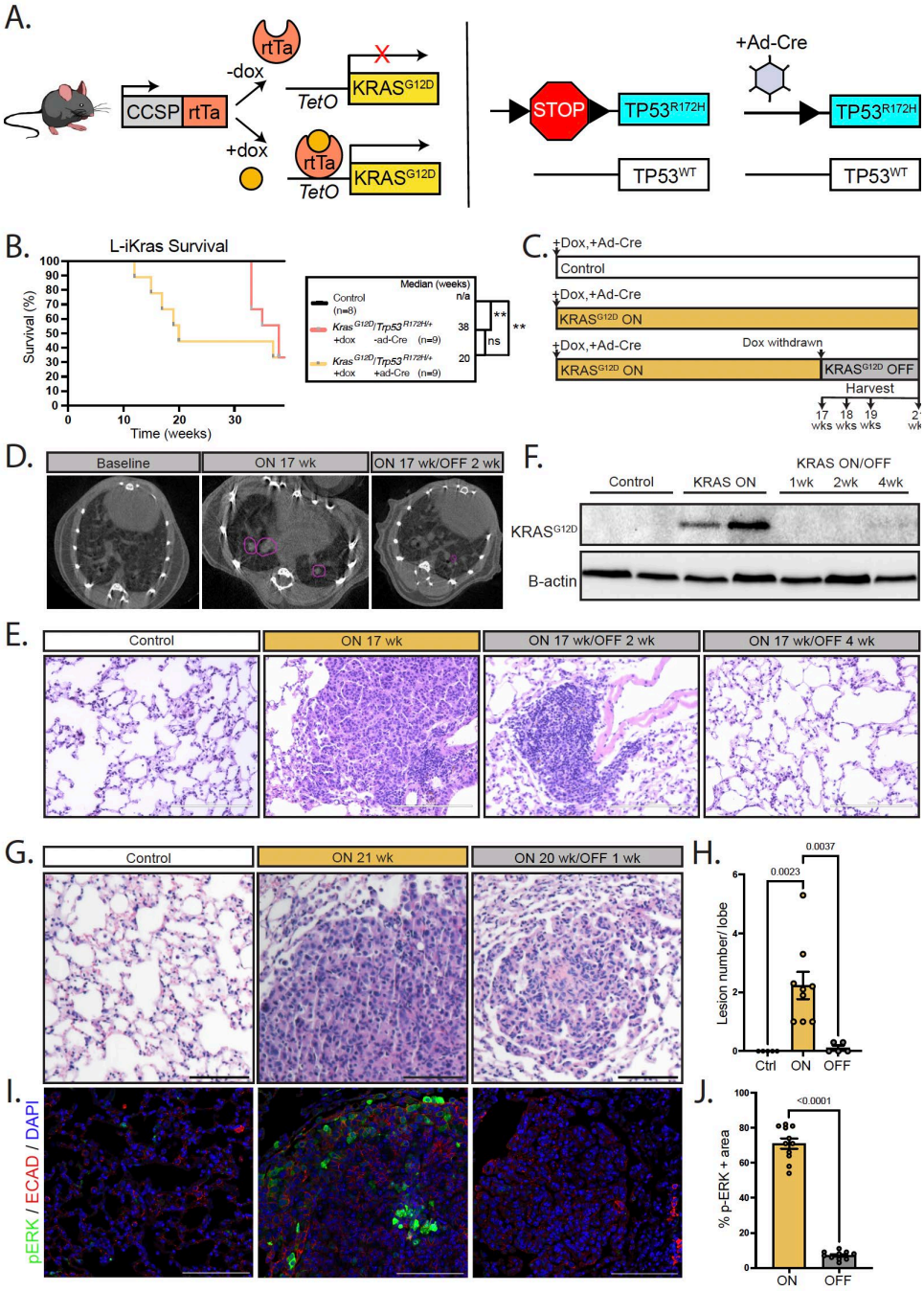

Figure 1. Inducible and reversible L-iKras mouse model of lung adenocarcinoma: (A) Genetic makeup of the L-iKras* mouse model: *CCSP*-rtTa; TetO-*Kras*^{G12D}; *Trp53*$^{LSL\text{-}R172H/+}$. **(B)** Kaplan-Meier survival curves for L-iKras mice**.** Control (n=8), *CCSP*-rtTa; TetO-*Kras*^{G12D}; *Trp53*$^{-/+}$ (n=9), *CCSP*-rtTa; TetO-*Kras*^{G12D}; *Trp53*$^{LSL\text{-}R172H/+}$ (n=9). Log-rank (Mantel-Cox) test, p = 0.0097. **(C)** Experimental design: ad-Cre and doxy were administered to induce *Trp53*^{R172H} and *Kras*^{G12D} expression in lung tissue. Doxy was withdrawn 17 weeks to reverse *Kras*^{G12D} expression. Mice were sacrificed and lungs were harvested at 17, 18, 19, 21 weeks after study start. Controls include mice lacking TetO-*Kras*^{G12D} or *CCSP*-rtTa cassettes, and mice with wildtype background. **(D)** Representative axial slices from CT scans of L-iKras mice at indicated time points. **(E)** Representative images of H&E stains of control and L-iKras lungs for indicated time points. Scale bar = 200 µM. **(F)** Western blot of Kras^{G12D} protein expression in L-iKras lung tissue harvested at indicated timepoints. **(G)** Representative images of H&E staining of control and L-iKras lungs at the indicated time points. Scale bar = 100 µM. **(H)** Quantification of lesions in H&E stained lung sections from L-iKras and control mice with and without doxy withdrawal. Data represent mean ±SEM. Statistical analyses determined by one-way ANOVA with post-hoc Tukey HSD test. **(I)** Representative IF staining for phospho-ERK (green), E-cadherin (red), and DAPI (blue) in L-iKras lung tissue at indicated timepoints. Scale bar = 100 µM. **(J)** Quantification of % area of p-ERK+ cells per tumor area. Data represent mean ±SEM. Statistical analysis determined by unpaired T test.

not found to be statistically significant when compared to mice expressing Kras^{G12D} alone, the observed trend may indicate an increase in disease severity when Trp53 is co-mutated, or the transition from adenomas to adenocarcinomas (**Figure 1B**). To investigate the effect of Kras^{G12D} inhibition on tumor growth, we conducted a study in which L-iKras "ON" mice and control littermates ("Control") were given ad-Cre and dox water for 17-21 weeks. A second group of L-iKras mice, the "OFF" group, were given ad-Cre for 17 weeks before dox withdrawal for 1, 2, or 4 weeks (**Figure 1C**). To monitor tumor growth, longitudinal and non-invasive micro-CT imaging was performed on the lungs of all experimental mice. Representative axial pulmonary CT images shown in **Figure 1D** indicate that Control mice showed no pulmonary lesions at 17 weeks, whereas triple transgenic mice "ON" dox showed pulmonary lesions at 17 weeks as indicated by purple circles. The representative CT image of the same mouse shown in the ON group, but two weeks post-dox withdrawal, shows that pulmonary lesions disappear, likely because of apoptotic cell death previously described by Fisher et al. [9]. Next, lungs were harvested from all experimental cohorts to assess tumor growth, Kras^{G12D} and surrogate pERK expression by western blotting or IHC. Overall lesions gradually decreased with dox withdrawal and were absent in H & E staining at 4 weeks post Kras^{G12D} depletion (**Figure 1E**). As expected, Kras^{G12D} expression was detected only in lung tissue from the ON group as assessed by western blotting using a RasG12D specific antibody (**Figure 1F**). Furthermore, the total number of lesions per lobe decreased statistically significantly when Kras^{G12D} expression was reversed by dox removal for 1-4 weeks (**Figure 1G, 1H**). As ERK phosphorylation is a surrogate marker for Kras^{G12D} signaling and indicative of Kras^{G12D} activity, we probed lung tissue sections from Control, ON, and OFF groups for ERK phosphorylation using immunofluorescent staining and confocal microscopy. Remarkably, we observed strong ERK phosphorylation in the epithelial compartment in the ON group but not in

the OFF or Control groups, demonstrating that $Kras^{G12D}$ expression, and thus signaling, is abrogated after dox withdrawal (**Figure 1I**). $Kras^{G12D}$ activity, represented as percent area of positive phospho-ERK per tumor, was determined as a ratio of percent area positive for phospho-ERK signal over percent area positive for DAPI. To measure the difference in $Kras^{G12D}$ activity between the ON and OFF state for the L-iKras mouse model, we quantified percent tumor area positive for phospho-ERK for 2-4 tumors per mouse for ON and OFF groups. We observed a significant reduction of ERK phosphorylation in tumors from the OFF group compared to those from the ON group. To mechanistically determine the effects of $Kras^{G12D}$ expression and depletion, lung sections from all experimental cohorts were probed for Ki67, TUNEL and Ras^{G12D} by IHC, revealing a decrease in cell proliferation, an increase in apoptosis and a decrease in Ras^{G12D} expression in OFF lung tissue compared to ON (**Figure S1A-B**). In summary, we demonstrate that induction of $Kras^{G12D}$ and cooccurring mutant Trp53 expression in the lung produces highly proliferative lung tumors that can be reversed by depletion of $Kras^{G12D}$ expression, resulting in a decreased number of pulmonary lesions due to apoptotic cell death of tumor cells.

Oncogenic Kras results in Gene Expression Changes in Epithelial Cells and Fibroblasts in the Tumor Microenvironment. To better understand $Kras^{G12D}$ dependent changes occurring in the tumor microenvironment, we utilized single cell RNA sequencing (scRNAseq). We harvested the right inferior lobe of the lung from the ON (21 weeks) and the OFF (21 weeks ON, 1 week OFF) groups and samples were processed simultaneously to avoid batch effects. The processed scRNAseq dataset had a total of 14,005 cells – 9,090 from the ON group and 4,915 from the OFF group. Data were analyzed using the Seurat package in R (version 4.0.2) and visualized by uniform and manifold approximation and projection (UMAP) (**Figure 2A**). As shown in **Figure 2B**, clusters from the ON and OFF groups overlayed sufficiently, indicating that similar cell types are

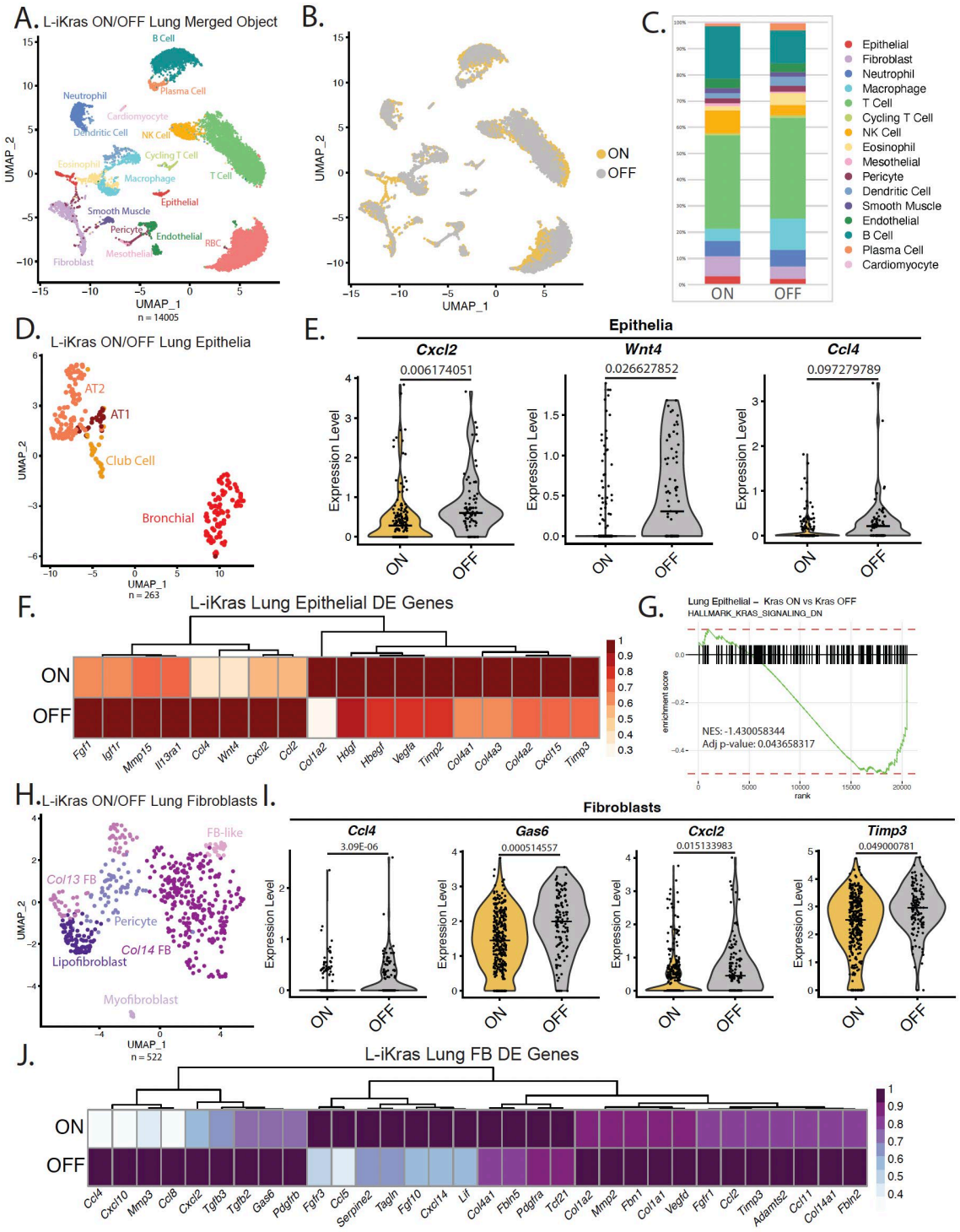

Figure 2. Oncogenic Kras changes epithelial and fibroblast gene expression in the tumor microenvironment: **(A)** UMAP visualization of scRNAseq data showing unsupervised clustering of cells from L-iKras lung samples (Kras ON – 21 weeks ON DOX, Kras OFF – 20 weeks ON + 1 week OFF). Each color represents a distinct cell cluster. **(B)** UMAP visualization of scRNAseq data showing overlap of Kras ON and Kras OFF groups. **(C)** Bar graph comparing cell cluster breakdown per sample (red blood cells were removed). **(D)** UMAP visualization of defined lung epithelial clusters from Kras ON and Kras OFF samples. **(E)** Violin plots of *Cxcl2*, *Wnt4*, and *Ccl4* comparing expression levels between total epithelial cells from Kras ON and Kras OFF samples. Adjusted p-value given above each violin plot. Median expression is marked. **(F)** Heatmap showing averaged scRNAseq expression data (relative to the highest expressor) for genes in epithelial cells curated from the differential gene expression list. **(G)** GSEA plot of Kras ON vs Kras OFF lung epithelia showing the running enrichment score for the 'HALLMARK_KRAS_SIGNALING_DN' gene set. NES = -1.430058344. Adjusted p-value = 0.043658317. **(H)** UMAP visualization of scRNAseq data showing unsupervised clustering of subsetted fibroblasts from Kras ON and Kras OFF samples. **(I)** Violin plots of *Ccl4*, *Gas6*, *Cxcl2*, and *Timp3* comparing expression levels between total epithelial cells from Kras ON and Kras OFF samples. Adjusted p-value given above each violin plot. Median expression is marked. **(J)** Heatmap showing averaged scRNAseq expression data (relative to the highest expressor) for genes in fibroblasts (pericytes removed) curated from the differential gene expression list.

present in both groups. Of note, we observed a higher percentage of fibroblasts in the ON compared to the OFF group and a higher percentage of macrophages in the OFF compared to ON group (**Figure 2C**). To better parse out differences between groups in the lung epithelia, epithelial cells were subclustered separately and visualized by UMAP (**Figure 2D**). We assessed changes in gene expression in the lung epithelia; interestingly, genes upregulated in the OFF group included chemokines *Cxcl2* and *Ccl4*, *Wnt4*, a non-canonical WNT signaling ligand, growth factor *Fgf1*, and the extracellular matrix remodeling factor *Timp3*. Genes upregulated in the ON group included *Vegfa* and *Cxcl15* (**Figure 2E-F, S2A**). We also assessed gene expression changes for genes known to change during lung cancer progression, including *Cxcl1*, *Tgfa*, and *Tgfb1*. While *Cxcl1* expression was upregulated in the OFF group, *Tgfa* expression was higher in the ON group, and *Tgfb1* expression showed no change (**Figure S2B**). Using gene set enrichment analysis (GSEA) we confirmed that Kras signaling was efficiently abrogated in the OFF group, as the "HALLMARK_KRAS_SIGNALING_DN" gene set, a list of genes that are downregulated upon Kras expression, was significantly upregulated in the OFF group (**Figure 2G**). Conversely, the "HALLMARK_KRAS_SIGNALING_UP" gene set, a list of genes that are upregulated upon Kras expression, trended up in the ON group (**Figure S2C**).

To obtain mechanistic insight into fibroblast reprogramming, we first subclustered the fibroblast population and visualized it by UMAP (**Figure 2H**). Fibroblasts were subclustered by comparing transcription of marker genes according to current literature [16, 17] (**Figure S2D-E**). Next, we looked at the transcriptional differences between the ON and OFF groups through differential expression. Differentially expressed genes included cytokines and growth factors including *Ccl4, Cxcl2, Tgfb,* and *Cxcl14*; extracellular matrix remodeling components including *Timp3, Col4a1,* and *Fbln5*; and Growth Arrest Specific 6 (*Gas6*), which is known to be

upregulated during growth arrest [16, 17] (**Figure 2I-J, S2F**). Given the driver mutation in our mouse model, we also looked at genes that are upregulated in fibroblasts in $Kras^{G12D}$-driven pancreatic cancer [18]. Interestingly, *Cxcl1* and *Il33* showed no change and *Il6* was upregulated in the OFF group, in contrast to what is seen in pancreatic cancer, indicating an environmental difference despite the same driver mutation (**Figure S2G**).

Oncogenic Kras Regulates Myeloid Cells in the Microenvironment of Lung Adenocarcinoma. To understand how oncogenic Kras affects immune cells in the TME, we queried the single cell RNA sequencing data and interrogated changes in myeloid cell composition by expression and visualized this by UMAP (**Figure 3A**). Specifically, *C1qa*, *C1qb*, and *C1qc*, which have been identified as immunosuppressive macrophage markers in pancreatic cancer [19], were all upregulated in the ON compared to the OFF group (**Figure 3B, Figure S3A**). Interestingly, *Apoe*, another marker of immunosuppression, was upregulated in the OFF group (**Figure 3C**), potentially indicating a mechanism of resistance. However, *Mrc1*, the gene encoding for CD206, and *Csf1r* were both upregulated in the ON group, suggesting that overall, macrophages exhibit an immunosuppressive phenotype in this group (**Figure 3C**). Macrophages showed transcriptional changes, indicating increased immunosuppression upon oncogenic Kras expression based on differential expression analysis (**Figure 3D**). Next, we interrogated differential expression changes in neutrophils and found that neutrophils in the OFF group showed an increase in both cytokines such as *Ccl3* and polarization markers such as *Cd274* and *Icam1* (**Figure 3E-G**). Interestingly, *Ccl3* and *Icam1* are markers of antitumoral neutrophils, whereas *Cd274* is a marker of activated neutrophils, indicating that when oncogenic Kras is turned ON, neutrophils are reprogrammed to be less antitumoral. This may potentially provide insight into efficacy of ICI therapies with Kras inhibitors.

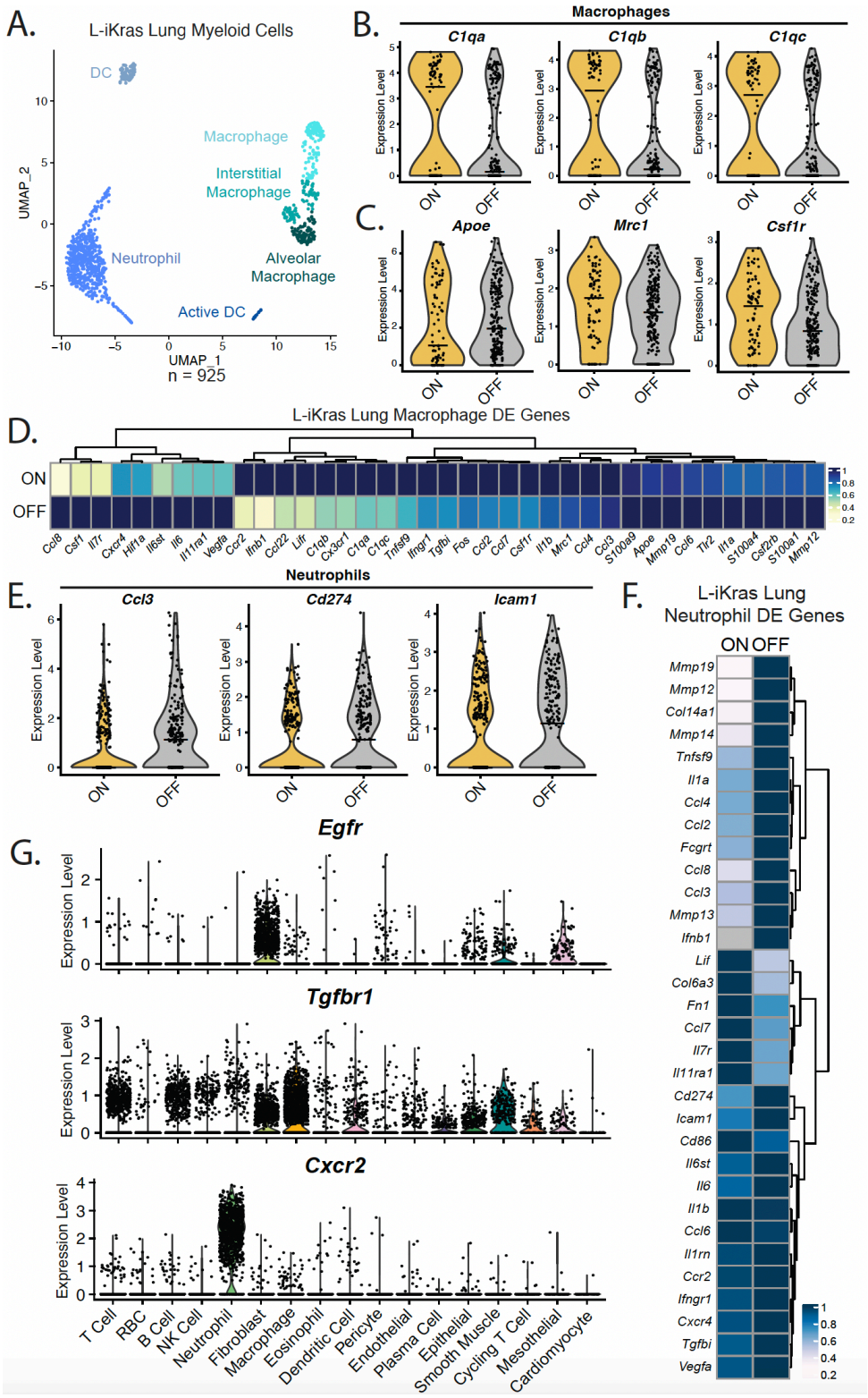

Figure 3. Oncogenic Kras regulates myeloid compartment of the lung adenocarcinoma microenvironment: (A) UMAP visualization of scRNAseq data showing unsupervised clustering of subsetted myeloid cells from Kras ON and Kras OFF samples. **(B-C)** Violin plots of *C1qa*, *C1qb*, *C1qc*, *Apoe*, *Mrc1*, and *Csf1r* comparing expression levels between macrophages from Kras ON and Kras OFF samples. Median expression is marked. **(D)** Heatmap showing averaged scRNAseq expression data (relative to the highest expressor) for genes in macrophages (combined macrophages, interstitial macrophages, and alveolar macrophages) curated from the differential gene expression list. **(E)** Violin plots of *Ccl3*, *Cd274*, and *Icam1* comparing expression levels between neutrophils from Kras ON and Kras OFF samples. Median expression is marked. **(F)** Heatmap showing averaged scRNAseq expression data (relative to the highest expressor) for genes in neutrophils from differential gene expression list. **(G)** Violin plots showing expression *Egfr, Tgfbr1* and *Cxcr2* across all identified cell populations in both Kras ON and Kras OFF samples combined.

Epithelial Kras^{G12D} Secretome affects Fibroblasts. To validate our *in vivo* findings from single cell RNA sequencing, we established *ex vivo* conditioned media experiments utilizing a L-iKras primary lung cancer cell line (LC3-547) generated from a pulmonary tumor from the ON group (**Figure 4A**). Induction and inhibition of Kras^{G12D} expression in lung cancer cells derived from the L-iKras model were confirmed by culturing cells in dox-containing media to sustain expression of Kras^{G12D}, and by removing dox from the media to inhibit its expression, respectively. Western blot analysis of protein lysates from both groups showed Kras^{G12D} protein expression persisted in dox-treated cells and diminished upon dox withdrawal (minus dox). The human KRAS^{G12D}-expressing lung cancer cell line A549 was used as a negative control to demonstrate antibody specificity of the Ras^{G12D} antibody (**Figure 4B**). While we showed that induction and inhibition of Kras^{G12D} expression can be achieved at the transcriptional level in cells derived from L-iKras mice, we also tested a clinically relevant and commercially available KRAS^{G12D} inhibitor, MRTX1133, to confirm our findings and assess clinical relevance. LC3-547 cells cultured in their regular media containing dox were treated with MRTX1133, hereafter denoted as MRTX. As seen in **Figure 4C**, Kras^{G12D} GTPase activity was found to be inhibited, as surrogate phosphorylation of ERK was markedly reduced upon MRTX treatment and comparable to that observed in minus dox treated cells. Next, we evaluated whether Kras^{G12D} expression in the L-iKras derived cells driven from the transgenic locus (TRE-Kras^{G12D}) is comparable to Kras^{G12D} expression driven from an endogenous locus in cells derived from the KP mouse model [20]. As seen in **Figure S4A**, KPL-86 cells derived from KP pulmonary tumors exhibit similar Kras^{G12D} expression and downstream signaling as assessed by western blot using RasG12D and phospho-ERK1/2 antibodies. Furthermore, KrasG12D expression and downstream ERK phosphorylation was inhibited in both lung cancer cells lines with MRTX (**Figure S4A**). To identify Kras^{G12D}-dependent secreted factors released

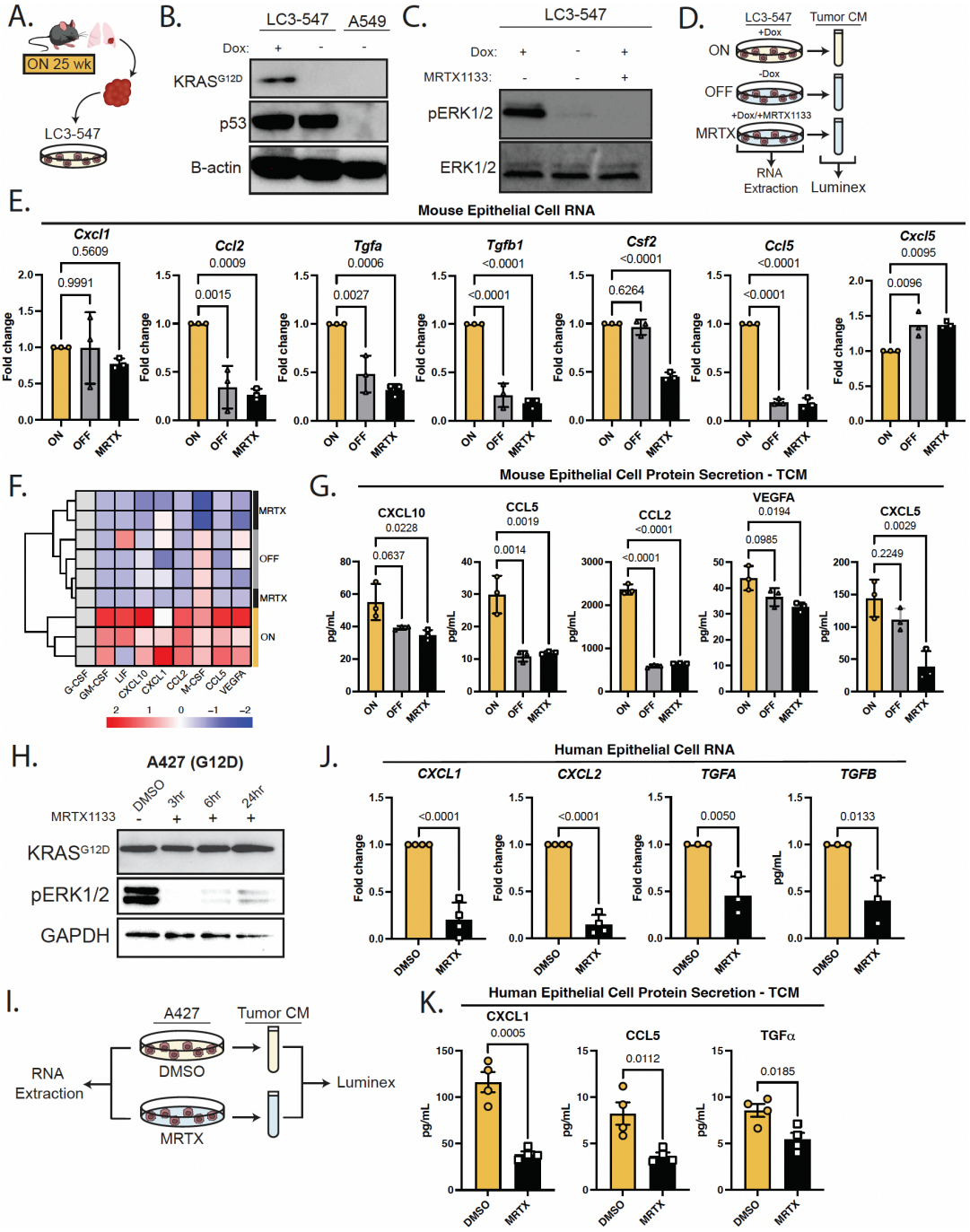

Figure 4. Immunosuppressive signatures are identified in epithelial Kras^{G12D} secretome: (A) Scheme of L-iKras cancer cell line, LC3-547, harvested from L-iKras lung tumor for subsequent *in vitro* experiments. **(B)** Western blot of Kras^{G12D} and p53 protein expression in LC3-547 cell line cultured with dox and after dox is withdrawn. **(C)** Western blot of reduced ERK phosphorylation in LC3-547 upon dox withdrawal or treatment with MRTX1133. **(D)** Experimental design. RNA was extracted from L-iKras cancer cells cultured with dox to activate Kras^{G12D} expression (ON) or dox was withdrawn (OFF) to turn off Kras^{G12D} expression, or cultured with dox and MRTX1133 (MRTX) to pharmacologically inhibit Kras^{G12D} GTPase activity. Tumor conditioned media was harvested for Luminex analysis. **(E)** Quantitative reverse-transcription polymerase chain reaction for *Cxcl1, Ccl2, Tgfa, Tgfb1, Csf2, Ccl5*, and *Cxcl5* expression in L-iKras cancer cells from ON, OFF, and MRTX treatment groups. **(F)** Heatmap of extracellular cytokines using Luminex assay generated from L-iKras tumor CM compared across ON, OFF, and MRTX treatment groups. **(G)** Quantification of CXCL10, CCL5, CCL2, VEGFA, CXCL5 cytokine levels in Luminex assay from L-iKras tumor CM. **(H)** Western blot of Kras^{G12D} expression and activity in human Kras^{G12D} lung adenocarcinoma cell line, A427, upon treatment with MRTX1133 for indicated time points. **(I)** Experimental design. RNA was extracted from human Kras^{G12D} cancer cells cultured with DMSO control or MRTX1133. Tumor conditioned media was harvested for Luminex analysis. **(J)** Quantitative reverse-transcription polymerase chain reaction for *CXCL1, CXCL2, TGFA, TGFB* expression in A427 cells from control and MRTX treated groups. **(K)** Quantification of CXCL1, CCL5, and TGFa cytokines generated from A427 tumor CM compared across DMSO (TCM) and MRTX treatment groups.

from tumor/epithelial cells into the microenvironment, we cultured L-iKras cancer cells with dox ('ON'), withdrew dox ('OFF'), or treated cells with MRTX. Cells from all groups were cultured for 48 hours before tumor conditioned media (TCM) was collected, and RNA extracted from the remaining cell pellets (**Figure 4D**). Our data show that *Ccl2, Tgfa, Tgfb1, Csf2,* and *Ccl5*, but not *Cxcl1* and *Cxcl5*, were differentially expressed in a $Kras^{G12D}$-dependent manner in LC3-547 cells utilizing qRT-PCR (**Figure 4E**). Multiplex ELISA (Luminex) assays performed on TCM from ON, OFF, and MRTX-treated cells revealed decreased cytokine levels in MRTX and OFF media conditions (**Figure 4F**). Notably, CXCL10, CCL5, CCL2, VEGFA, and CXCL5, but not CXCL1 and M-CSF cytokine secretion were found to be $Kras^{G12D}$-dependent, as they decreased in $Kras^{G12D}$ depleted or inhibited cell conditioned media (**Figure 4G, Figure S4B**). To recapitulate these findings in human lung cancer cells, the $KRAS^{G12D}$-mutant lung adenocarcinoma cell line A427 was treated with MRTX prior to collecting protein, RNA and TCM. As demonstrated in **Figure 4H**, A427 cells express $Kras^{G12D}$ and exhibit high levels of pERK, which were both markedly reduced when treated with MRTX. Furthermore, expression of *Tgfa, Tgfb1, Cxcl1* and *Cxcl5* was found to be reduced in MRTX-treated cells using qRT-PCR, as was the secretion of CXCL1, CCL5, and TGFα in Luminex assays (**Figure 4I-K**). Together, these data reveal an epithelial $Kras^{G12D}$-dependent secretome containing tumor promoting and immunosuppressive components.

Fibroblast derived factors regulate macrophages in a $Kras^{G12D}$-dependent manner. Next, we sought to investigate how the identified secreted factors affect fibroblasts. We first established a normal lung fibroblast cell line, NLF-2522, from a control mouse (**Figure 5A**). Next, NLF-2522 fibroblasts were cultured for 24 hours in TCM from ON, OFF, and MRTX treated LC3-547 cells prior to collecting conditioned media and harvesting RNA from cell pellets (see schematic in **Figure 5B**). The conditioned fibroblast media was termed 'cancer associated fibroblast

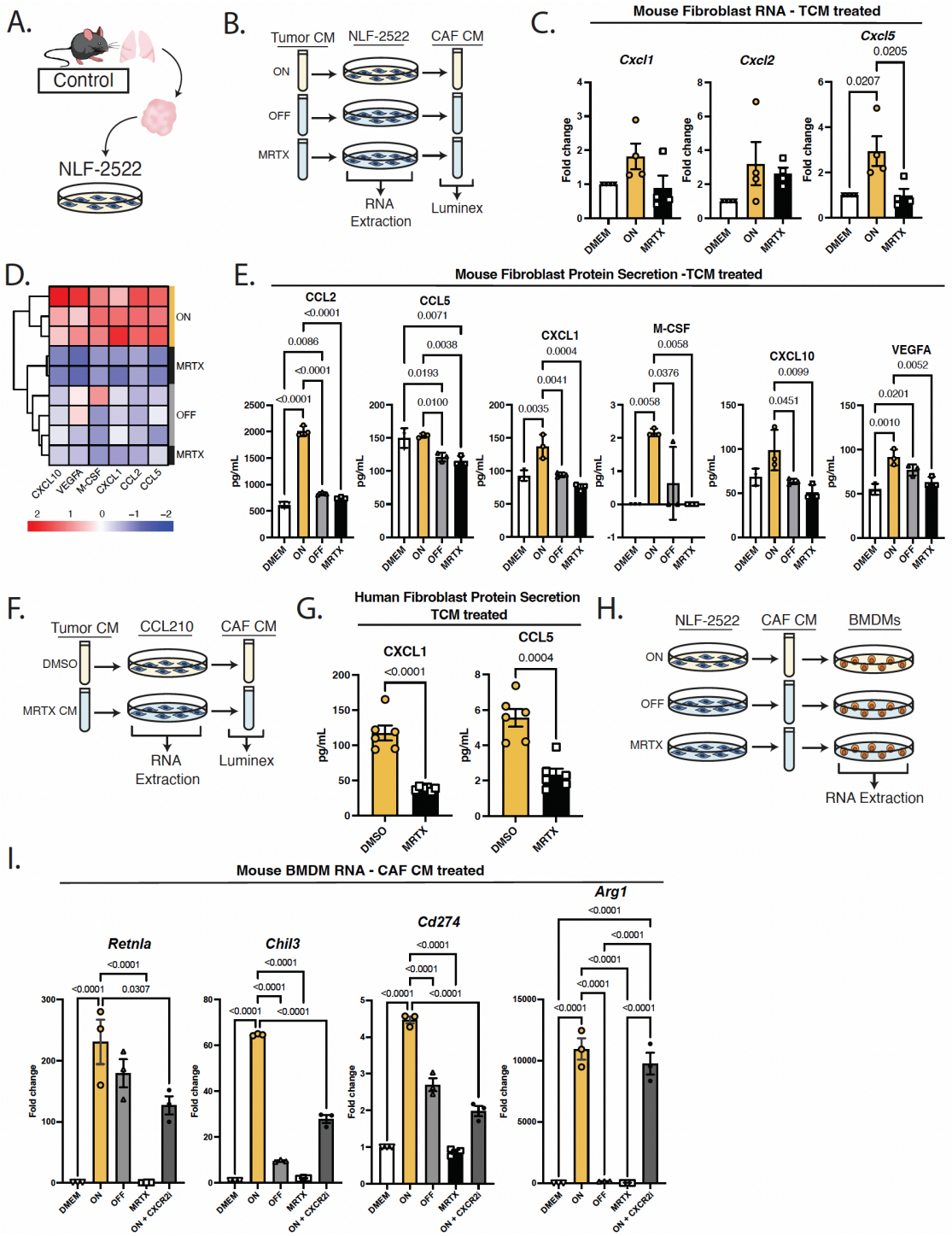

Figure 5. **Conditioned CAFs release immunosuppressive secretome that engages macrophages in a Kras^{G12D}-dependent manner: (A)** Scheme of normal lung fibroblast cell line, NLF-2522, harvested from L-iKras control mouse lung for subsequent *in vitro* experiments. **(B)** Experimental design. NLF-2522 fibroblasts were cultured in tumor CM from ON, OFF, MRTX, or DMEM with 1% FBS for control. RNA was extracted from fibroblasts. Luminex analysis was conducted on CAF CM. **(C)** Quantitative reverse-transcription polymerase chain reaction for *Cxcl1, Cxcl2, Cxcl5* expression in NLF-2522 fibroblasts from ON, MRTX, and DMEM and MRTX treatment groups. **(D)** Heatmap of extracellular cytokines generated from NLF-2522 CAF CM compared across ON, OFF, and MRTX treatment groups. **(E)** Quantification of CCL2, CCL5, CXCL1, M-CSF, CXCL10, VEGFA cytokine levels in CAF CM. **(F)** Experimental design. Adult human lung fibroblast cells, CCL210, were cultured in tumor CM from A427 cells treated with MRTX or DMSO control. RNA was extracted from conditioned CCL210 cells and Luminex analysis was conducted on CAF CM. **(G)** Quantification of CXCL1 and CCL5 cytokine levels in human CAF CM. **(H)** Experimental design. Bone marrow derived macrophages (BMDM) were cultured in CAF CM from ON, OFF, MRTX, and DMEM groups. RNA was extracted from BMDM. **(I)** Quantitative reverse-transcription polymerase chain reaction for M2 markers: *Retnla, Chil3, Cd274, Arg1* expression in treated BMDMs from ON, OFF, MRTX, and DMEM treatment groups.

conditioned media', hereafter referred to as 'CAF CM'. qRT-PCR was performed to validate differential expression of selected immunosuppressive markers identified in scRNAseq analysis of fibroblast subpopulations (see **Figure 2J**). Interestingly, *Cxcl5*, but not *Cxcl1* and *Cxcl2* gene expression was regulated in a $Kras^{G12D}$-dependent manner in the fibroblasts (**Figure 5C**). Furthermore, Luminex analysis of CAF CM revealed distinct clustering of secreted cytokines and growth factors in 'MRTX' and 'OFF' CM when compared to 'ON' CM (**Figure 5D**). Notably, CCL2, CCL5, CXCL1, M-CSF, CXCL10, and VEGFA secretion appeared to be $Kras^{G12D}$-dependent, as they decreased with $Kras^{G12D}$ inhibition (**Figure 5E**). To recapitulate our findings in a relevant human *ex vivo* system, we generated TCM from $Kras^{G12D}$-mutant A427 cells as described above. Next, we incubated an adult human lung fibroblast cell line, CCL210, in TCM from A427 cells that either were treated with MRTX or left untreated, to generate human CAFs and CM (**Figure 5F**). Conditioned media (CAF CM) was collected for secretome analysis of candidate cytokines and cells were pelleted to obtain RNA for gene expression studies. Surprisingly, gene expression of *Cxcl5*, *Cxcl1* and *Cxcl2* did not change in human CAFs incubated with TCM from untreated or MRTX-treated A427 cells (**Figure S5A**), but secretion of CXCl1 and CCL5 cytokines using Luminex analysis was found to be $Kras^{G12D}$-dependent. In fact, we observed a statistically significant reduction in CXCl1 and CCL5 release upon $Kras^{G12D}$ inhibition (**Figure 5G**). To investigate whether TGFα signaling stemming from epithelial cells is required for fibroblast activation measured by *Cxcl 1,2,5* expression, NLF-2522 fibroblasts were cultured in ON, OFF, or MRTX TCM. In addition, NLF-2522 cells conditioned with ON TCM were treated with an EGFR inhibitor, Erlotinib, to investigate whether TGF signaling from epithelial cells can be disrupted by blocking its cognate receptor (EGFR) on fibroblasts. This group is denoted as the "ON+ EGFRi" group. Interestingly, EGFR inhibition resulted in statistically significant inhibition

of *Cxcl5,* but not *Cxcl1* and *Cxcl2* expression, demonstrating that fibroblast activation is dependent on epithelial TGFα and requires $Kras^{G12D}$ expression (**Figure S5B**).

To understand the consequence of $Kras^{G12D}$-dependent CXCL1 and 5 secretion from CAFs, we established another *ex vivo* system utilizing bone marrow derived macrophages (BMDM). CXCL1 and 5 are factors known to regulate myeloid recruitment, activation, and polarization. To assess the possible role of $Kras^{G12D}$-mediated CAF cytokine secretion on polarization of macrophages, we isolated and differentiated BMDMs from control mice and cultured them in CAF CM from ON, OFF and MRTX-treated fibroblasts for six days (**Figure 5H**). Gene expression analysis performed on conditioned macrophages revealed a statistically significant upregulation of established tumor associated macrophage (TAM) markers *Arg1*, *Rentl1a, Chil3* and *Cd274* [21, 22] when BMDMs were cultured in ON CAF CM compared to those conditioned in DMEM-control media. Moreover, the expression of immunosuppressive TAM M2-like markers was dramatically reduced when BMDMs were cultured in OFF and MRTX CAF CM (**Figure 5I**). To determine the relevance of CXCL signaling on macrophage polarization to TAMs, BMDMs were incubated with ON CAF CM supplemented with an inhibitor against the cognate receptor for CXCL1, 2 and 5 (CXCR2, SB225002) (**Figure 5I**). Treatment with CXCR2 inhibitor SB225002 significantly prevented TAM marker expression but did not abrogate expression entirely as seen with MRTX, indicating that CXCL1, 2 and 5 are not the sole factors regulating polarization of macrophages to TAMs (**Figure 5I**). In summary, our data suggest a mechanism by which CAFs mediate immunosuppression through CXCL 1, 2 and CXCL 5 signaling in a $Kras^{G12D}$-dependent manner, as signals stemming from epithelial cells expressing oncogenic Kras are required to activate fibroblasts.

Kras^{G12D}-dependent cross talk between epithelial cells, fibroblasts and myeloid cells is recapitulated in human lung adenocarcinoma. To assess the clinical relevance of our findings in the Kras inducible and reversible lung adenocarcinoma mouse model, we used a publicly available scRNAseq dataset of KRAS^{G12D}-driven and non-KRAS-driven lung cancer [1]. We analyzed the data similarly to our mouse scRNAseq dataset (**see Figure 2A**), but included batch correction for patients using Seurat's IntegrateData pipeline [23]. The dataset was visualized using UMAP (**Figure 6A**). To recapitulate crosstalk between the different cell types found in the tumor microenvironment of murine lung cancer, we filtered scRNAseq data for expression of known signaling pairs as previously done in our lab [24]. We identified significant predicted interactions upregulated in KRAS^{G12D}-driven lung cancer (**Figure 6B**) indicating that epithelial cell and macrophage signaling were changing the most. Differential expression analysis of epithelial cells showed a significant increase in expression of *CXCL1*, *CXCL2*, and *HDGF* in the KRAS^{G12D}-driven lung cancer samples when compared to non-KRAS-driven lung cancer (**Figure 6C-D**). Furthermore, in macrophages, we observed a significant increase in expression of C1QB and C1QC in KRAS^{G12D}-driven, but not non-KRAS-driven lung cancer, recapitulating our findings in the L-iKras model (**Figure 6E-F**). Although the number of fibroblasts in the human samples was limited, some *in vitro* data were corroborated, including the increased expression of CXCL1 in the KRAS^{G12D} lung cancer samples versus the non-KRAS-driven samples (**Figure S6A**), providing potential targets in the TME for future studies evaluating co-targeted approaches with KRAS inhibitors.

In summary, our findings provide mechanistic insight into the extrinsic signaling consequences of oncogenic Kras in lung cancer. We have identified a KrasG12D secretome that regulates and activates fibroblasts, which in turn recruit, activate and polarize myeloid cells to

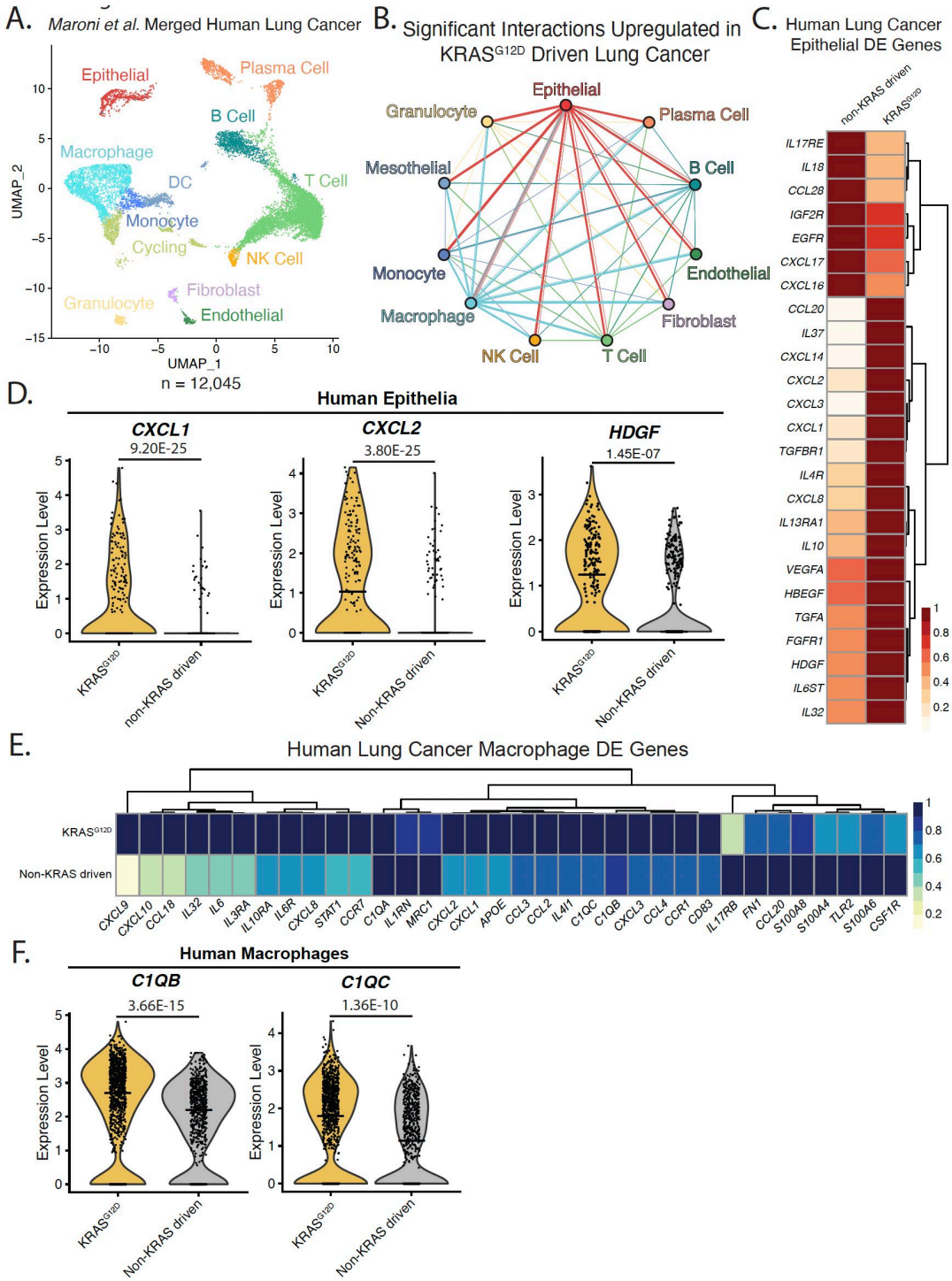

Figure 6. scRNAseq analysis of human lung adenocarcinoma recapitulates gene expression of distinct immunosuppressive markers from L-iKras epithelial and fibroblast secretomes: (A) UMAP visualization of scRNAseq data showing unsupervised clustering of cells from lung cancer samples. KRAS status either Kras^{G12D} or KRAS wild-type [1]. Each color represents a distinct cell cluster. **(B)** Interactome showing potential ligand/receptor pair interactions that are significantly (adjusted p-value <0.05) upregulated in the Kras^{G12D} driven lung cancer samples. **(C)** Heatmap showing averaged scRNAseq expression data (relative to the highest expressor) for genes in epithelial cells curated from the differential gene expression list. **(D)** Violin plots of *CXCL1, CXCL2,* and *HDGF* comparing expression levels between total epithelial cells from Kras^{G12D} vs KRAS-wt samples. Adjusted p-values given above each violin plot. Median expression is marked. **(E)** Heatmap showing averaged scRNAseq expression data (relative to the highest expressor) for genes in human macrophages [1] curated from the differential gene expression list. **(F)** Violin plots of *C1QB* and *C1QC* comparing expression levels between total epithelial cells from Kras^{G12D} vs KRAS-wt samples. Adjusted p-value given above each violin plot. Median expression is marked.

provide a tumor promoting, immunosuppressive microenvironment. Our data further provide factors that are upregulated in response to KRAS inhibitors, potentially indicating relevant mechanisms of resistance.

Discussion

Oncogenic mutations in the *KRAS* gene are a hallmark feature of many cancer types, including a subset of non-small cell lung cancer (NSCLC) [2]. With the advent of isoform-specific mutant Kras inhibitors, understanding how mutant Kras functions in the context of advanced disease is critical to prevent/overcome resistance to targeted treatment. Mutant Kras is a driver mutation for lung cancer [5]; further, it is required for tumor maintenance in a mouse model of the disease [9], indicating a cell autonomous role of oncogenic Kras in cancer cells. Less understood is the extrinsic effect of modulating oncogenic Kras on the tumor microenvironment. Here, we used Lung-iKras mice, leveraging inducible and reversible expression of oncogenic Kras in the lung epithelium, to interrogate how inactivating oncogenic Kras in established tumors alters components of the tumor microenvironment. Single cell RNA sequencing technologies allowed us to conduct in-depth characterization of cell types within tumors upon Kras inactivation. Our data show that Kras inactivation results in changes in the transcriptional program of fibroblasts. Specifically, cytokines such as *Ccl5, Cxcl14, Cxcl*15 and *Vegf* (an angiogenic factor) were downregulated upon Kras inactivation. In contrast, a different cytokine expression profile was activated that included *Ccl2, Ccl4, Ccl8* and *Cxcl10.* As the receptors for many of these cytokines are expressed by myeloid cells infiltrating the tissue, we sought to determine whether the latter also changed in response to oncogenic Kras inactivation. Analysis of the single cell RNA data revealed a clear change in macrophage polarization, consistent with a reduction in the immunosuppressive potential of the macrophages. The question then arose as to how Kras mutant cancer cells alter both fibroblast and macrophage polarization. We used *in vitro* approaches to investigate this in a simpler model: we generated Lung-iKras cancer cell lines and found that conditioned media from these cells induced activation of a cytokine program in cultured lung fibroblasts, similar to the *in vivo* findings. Thus, a direct link exists between cancer cells and

fibroblasts, mediated by a soluble factor that is transferred in the media. We then sought to determine which cancer cell might mediate crosstalk with fibroblasts. While we identified multiple factors that are secreted by cancer cells in a Kras-dependent manner, we were unable to identify which of these directly acted on fibroblasts.

Next, we used bone marrow derived macrophages to interrogate whether cancer cells could similarly induce macrophage polarization. However, culture with cancer cell conditioned mediums did not alter macrophage polarization. We then set up a system whereby fibroblasts were cultured with cancer cell conditioned media, followed by the transfer of the conditioned media from the fibroblasts to bone marrow derived macrophages. In this experiment, macrophages were repolarized, observed as expression of tumor associated macrophage (TAM) markers such as Arginase and C1Q. Further, treatment with an inhibitor for CXCR2, the receptor of fibroblast-derived cytokines such as Cxcl1 and Cxcl5, partially abrogated activation of these TAM markers.

Overall, our data support the notion that, in lung cancer, Kras activates a specific program inducing secretion of multiple cytokines and growth factors; in turn, these factors reprogram fibroblasts to regulate macrophage polarization. The net effect of oncogenic Kras activation is thus the establishment of a complex and largely immunosuppressive microenvironment. Interestingly, inactivation of oncogenic Kras also drives expression of multiple cytokines that are likely involved in tissue repair but also possibly provide a niche for cancer cells; this might lead to tumor relapse and should be investigated in future studies.

While the cell autonomous effects of oncogenic Kras are well characterized, an emerging body of literature is now also describing its extrinsic effects. In pancreatic cancer, a $Kras^{G12D}$-driven malignancy [25], oncogenic Kras drives macrophage and fibroblast reprogramming; however, the cytokine profile of fibroblasts exposed to cancer cell secreted factors is drastically

different than what we found in the lung [18]. An extrinsic, oncogenic Kras secretome has been recently described in Kras mutant colorectal cancer [26], also with distinct characteristics. It is possible that organ-specific differences explain the clinical outcomes of these diseases, including varied responses to immunotherapy.

KRAS mutations are common in non-small cell lung cancer (NSCLC) and are often concurrent with TP53 mutations. Although the KRAS oncogene was once considered 'undruggable,' the FDA approval of the $KRAS^{G12C}$ inhibitor Sotorasib in 2021 [27-29] gave patients with the G12C mutation a viable treatment option. Inhibitors for other KRAS mutations have also shown tumor control in preclinical testing and are entering clinical trials, including the $KRAS^{G12D}$ inhibitor MRTX1133 [30]. In fact, clinical use of MRTX1133 is expected to be paradigm shifting for the treatment of NSCLC patients whose tumors bear the G12D mutation: approximately 56% of never smokers and 14% of smokers [31]. Moreover, since 30% of NSCLC patients respond to immunotherapy, the efficacy of combining $KRAS^{G12D}$ inhibitors with immune checkpoint immunotherapy (ICI) is expected to increase. At the same time, resistance to molecularly targeted therapies—and therefore relapse—is common. This has been observed with Sotorasib [4, 7] and there is concern that resistance to MRTX1133 and other KRAS inhibitors will also develop. Intriguingly, resistance mechanisms are often linked to remodeling of the tumor microenvironment [7]. Thus, the need to understand the remodeling process of the tumor microenvironment during intervention and tumor recurrence has emerged, to guide the development of future therapeutic treatment paradigms with long-term responses.

Considerable heterogeneity in lung cancer has prevented efficacy of new targeted immune therapies, with only ~11% of all lung cancer patients respond to ICI therapy. Recent single cell sequencing studies in human lung adenocarcinoma and murine KP models provide some insight

into not only the heterogeneity of tumors but also the composition of the tumor microenvironment [1, 16]. Specifically, tumor-infiltrating immune cells, fibroblasts and endothelial cells have been described as contributors to a distinct subpopulation of lung adenocarcinoma and likely drive its progression. In accordance with some of our findings, Kim et al. has described molecular and cellular reprograming of metastatic lung adenocarcinoma and how stromal and immune interactions result in a pro-tumoral and immunosuppressive microenvironment, which likely drives progression to metastatic disease [16]. Furthermore, this study described how lung resident myeloid cells were gradually replaced with monocyte-derived macrophages and dendritic cells during progression, along with increased T-cell exhaustion [16]. Our studies provide insight into the gene expression changes initiated upon Kras activation that result in the activation of cancer associated fibroblasts in the surrounding stroma. Growth factors such as TGFα and TGFβ have long been described as important factors in lung tumor growth, but until now, were not determined to be Kras dependent. Furthermore, activation of fibroblasts can be prevented utilizing an EGFR inhibitor, showing the importance of the interaction between epithelial cells and fibroblasts. Activation of fibroblasts in turn results in expression and secretion of factors like CXCL1, 2 and 5, which are known to recruit and polarize macrophages, but not in a Kras-dependent manner. Inhibition of the receptor for these cytokines using a CXCR2 inhibitor provides further insight into the importance of fibroblast dependent immune polarization. Our study thus provides mechanistic insight into how KrasG12D drives tumorigenesis in the lung and identifies potential actionable factors that could be utilized to target the tumor microenvironment in lung cancer.

In summary, with the increased clinical use of KRAS inhibitors, resistance is anticipated, and its mechanisms need to be understood to provide long-term benefits for lung cancer patients. Very few mechanistic studies have interrogated the changes in the tumor microenvironment upon

KRAS inactivation or inhibition. Our study provides a first look at the changes occurring in the tumor microenvironment upon both activation and inactivation of oncogenic Kras, including the role of fibroblasts and immune cells in the remodeling process. The Lung-iKras mouse provides a murine model system that allows for further interrogation of these observed changes to predict mechanisms of resistance and to provide co-targeted strategies for future use with KRAS inhibitors. Thus, our findings provide rationale to co-target changes in the tumor microenvironment for preventing resistance to KRAS inhibitors, which will guide precision medicine for lung cancer patients.

Materials and Methods

Mice

Mice were housed in a pathogen-free facility at the University of Michigan and overseen by the Unit for Laboratory Animal Medicine (ULAM). All animal studies were conducted in accordance with the University of Michigan's Institutional Animal Care and Use Committee guidelines approved protocol PRO00010349. Briefly, male and female mice with *CCSP*-rtTa and TetO-*Kras*^{G12D} cassettes, first described by the Varmus laboratory [9], were crossed with *Trp53*$^{LSL\text{-}R172H/+}$ described by the Jacks Laboratory [32] to generate a triple transgenic lung adenocarcinoma mouse model (L-iKras) with inducible expression of mutant Trp53 and inducible and reversible expression of mutant KrasG12D in club cells (lung epithelia). Combinations of single or double mutant littermates or wildtype were used as controls. ***Administration of doxycycline in drinking water:*** Expression of Kras^{G12D} was induced in female and male adult mice (8 weeks or older) through administration of doxycycline (Sigma, catalog number D9891) in drinking water at a concentration of 0.5 mg/ml and replaced every 2-3 days. Two different control groups were used to control for the effects of doxycycline on lung tissue and for leakiness of the TetO-*Kras*^{G12D}. Single transgenic control mice were given doxycycline in drinking water at the same dose as the experimental cohorts and triple transgenic mice were given water without doxycycline. ***Intranasal adenovirus-Cre instillation:*** Initiation and continued expression of *Trp53*^{R172H} mutant allele was achieved through administration of ad-Cre recombinase. Adenovirus-precipitate mixture was diluted in MEM media with 10mM $CaCl_2$ solution for a final titer of $3x10^7$ PFU/50 µL/mouse and delivered once, intranasally, at the study start date. Kaplan-Meier method and log-rank test were used to generate survival curves and test their difference. Bonferroni method was used to correct P values for pairwise comparisons.

Single cell RNA sequencing

We harvested the right inferior lobe of the lung for scRNAseq ON for 21 weeks (N = 2, pooled for submission) or ON for 20 weeks then OFF for 1 week (N = 2, pooled for submission). Each sample was harvested and processed simultaneously to avoid batch effects. In brief, lung tissues were mechanically minced and enzymatically digested with collagenase P (1 mg/mL in Roswell Park Memorial Institute (RPMI) 1640). Cell suspensions subsequently were filtered through 500 µm, 100 µm, and 40 µm mesh to obtain single cells. Dead cells were removed using the MACS Dead Cell Removal Kit (Miltenyi Biotec, Bergisch Gladbach, Germany). The resulting single-cell suspensions were pooled by experimental group (Kras ON/Kras OFF). Single-cell complementary DNA libraries were prepared and sequenced at the University of Michigan Advanced Genomics Core using the 10× Genomics Platform (raw and processed data will be made available through GEO database upon publication). Samples were run using 50-cycle, paired-end reads on the HiSeq 4000 (Illumina, San Diego, CA) to a depth of 100,000 reads. Raw data were processed and aligned by the University of Michigan DNA Sequencing Core. Cell Ranger count version 6.0.0 (10× Genomics, Pleasanton, CA) was used with default settings, with an initial expected cell count of 10,000. R version 4.2.1, RStudio version 2023.06.0+421, and R package Seurat version 4.0.2 were used for scRNAseq data analysis (RStudio Team, 2020). RStudio: Integrated Development for R. RStudio, PBC, Boston, MA URL http://www.rstudio.com/.; R Core Team (2023). _R: A Language and Environment for Statistical Computing. R Foundation for Statistical Computing, Vienna, Austria. <https://www.R-project.org/>.). Data initially were filtered to include only cells with at least 100 genes and genes that appeared in more than 3 cells. Data were normalized using the NormalizeData function with a scale factor of 10,000 and the LogNormalize normalization method. Data then were filtered manually to include only cells with 800–100,000 transcripts and

<15% mitochondrial genes. Variable genes were identified using the FindVariableFeatures function. Data were scaled and centered using linear regression of transcript counts. PCA was run with the RunPCA function using the previously defined variable genes. Cell clusters were identified via the FindNeighbors and FindClusters functions, using dimensions corresponding to approximately 90% variance as defined by PCA. UMAP clustering algorithms were performed with RunUMAP. Clusters were defined by user-defined criteria. The complete R script, including figure-specific visualization methods, is publicly available on GitHub (https://github.com/PascaDiMagliano-Lab).

Human single cell data were analyzed using the same methods using to analyze mouse data with the addition of Seurat's IntegrateData pipeline to mitigate batch effects [23]. GSE136246 pulled samples: 2 KRAS wild type patient tumors - total of 3 samples (NSC010.t1, NSC010.t2, NSC037) and 3 $KRAS^{G12D}$ mutant patient tumors - 6 samples (NSC016.t1, NSC016.t2, NSC016.t3, NSC020.t1, NSC020.t2, NSC036).

Interactome analysis was performed as described by Velez-Delgado et al. [18]. Ligand-receptor pairs were defined based on a curated literature-supported list described by Ramilowski et al. [33] and further curated as described by Steele et al. [34]. The average expression values of ligands and receptors in each cell population for both groups ($KRAS^{G12D}$/non-KRAS driven) were calculated individually, and ligands and receptors expressed below a user-defined threshold (median average expression) were removed from analysis. Ligand-receptor pairs also were excluded if the ligands and receptors were not expressed in both experimental groups. Differences in the ligands and receptors between groups were determined using the Wilcoxon rank test, and P values were adjusted for multiple comparisons using the Bonferroni correction method. Ligands and receptors were considered significantly different if $P < .05$. The resulting data table was visualized using

Cytoscape (version 3.7.2) software (https://cytoscape.org/) [35]. The complete R script is publicly available on GitHub (will be made available upon publication).

Histology and immunohistochemistry

Murine lungs were perfused in 1x PBS then fixed in 10% neutral-buffered formalin and stored in 70% ethanol before embedding in paraffin. The right lung lobe was used for histology and sent to the University of Michigan Histology Core for paraffin embedding, sectioning, and Hematoxylin and Eosin (H&E) staining. Additional sections were hybridized with Ki67 antibody and probed with Apoptag (TUNEL assay). Briefly, sections were deparaffinized and rehydrated then washed in deionized water for 2 minutes. Staining was performed with Harris hematoxylin solution, and counterstaining with eosin-phloxine solution, then sections were mounted with a Cytoseal XYL xylene-based mounting medium. Brightfield images (20X) were acquired with an Olympus BX-53 microscope, an Olympus DP80 digital camera, and Olympus cellSens standard software.

Immunofluorescence

RNA scope Multiplex Fluorescent Detection with Immunofluorescence: RNA scope multiplex fluorescent detection was preformed according to manufacturer's instructions (Advance Cell Diagnostics; ACD) and as previously described [36]. Briefly, 5 µm formalin fixed paraffin embedded lung tissue sections were mounted on charged slides and baked at 60°C for 1 hour. Sections were deparaffinized, dehydrated, and washed with RNAse-free 1x phosphate-buffered saline (PBST) three times, followed by incubation with hydrogen peroxide for 10 minutes at room temperature and target retrieval for 15 minutes at 98°C. Tissue sections were fixed with formalin and treated with ProteasePlus Reagent (ACD) for 15 minutes at 40°C. Amplification and signal

enhancement were performed for C1qa probe. C1qa probe was diluted per manufacturer's instructions and slides were incubated with them at 40°C for 2 hours. Slides were then washed twice with RNA scope washing buffer (ACD). Signal for the probe was amplified with AMP reagents horseradish peroxidase and tyramide signal amplification kit (ACD) at 40°C. Slides were then washed three times with 1x PBS before blocking with co-detection antibody diluent (ACD) for 30 minutes. Slides were then incubated with F4/80 and E-Cadherin primary antibodies (1:200 in co-detection antibody diluent) overnight at 4°C. The next day, slides were washed three times with 1x PBS then incubated with anti-rabbit secondary Fluor IgG (H+L) antibody (1:400 in co-detection antibody diluent for 1 hour at room temperature). Finally, slides were incubated with DAPI for 15 minutes at room temperature and washed 3 times with 1x PBS prior to being mounted with ProLong Diamond Antifade.

Multiplex TSA Immunofluorescent staining: Formalin-fixed, paraffin-embedded (FFPE) lung tissue sections (5-10 µm thick) were mounted on charged slides and baked at 60°C for 1 hour, deparaffinized, and dehydrated. Slides were then washed with deionized water for 2 minutes followed by antigen retrieval at 96°C in 10 mmol/L sodium citrate (pH 6.0) for 8 minutes. Once cooled to room temperature, slides were washed three times (2 minutes per wash) with 1x PBS and endogenous peroxides were quenched with 3% hydrogen peroxide for 15 minutes. The TSA kit (Invitrogen) was used per the manufacturer's guidelines. Briefly, slides were incubated with proprietary blocking serum provided in the kit then stained with antigen-specific primary antibodies overnight at 4°C: phospho-ERK (1:200), PDGFRb (1:100), aSMA (1:1000), F4/80 (1:200), ECAD (1:100). The following day, slides were washed three times with 1x PBS then incubated in anti-rabbit secondary antibody for 1 hour at room temperature. Slides were then washed three more times with 1x PBS. TSA conjugated to 488 or 555 fluorophores was applied

for 10 minutes, followed by incubation with a reaction stop reagent for 5 minutes. Finally, slides were incubated with DAPI for 5 minutes followed by three washes with 1x PBS prior to mounting with ProLong Diamond Antifade mounting solution. Antibodies used are listed in **Supplemental Table 1.**

Confocal Imaging: Entire lesion or normal lung tissue areas from ON, OFF, or Control groups were captured through high-magnification (40X) tile-scans on the Leica Stellaris 5 confocal microscope [37].

Confocal Image Analysis: Quantification of positive expression in tumor or normal lung area was performed using FIJI (National Institutes of Health, Bethesda, MD) by converting each channel from raw tiffs of ROI to 8-bit images with automatically set thresholds then inverting to 8-bit LUT. Percentage of the ROI positive in expression was measured for each channel (DAPI, aSMA, PDGFR, C1qa, F4/80, p-ERK, E-cadherin). Percentage of areas positive in p-ERK, PDGFR, or F4/80 were normalized to percentage area positive for DAPI. Percentage of areas positive for aSMA were normalized to percentage area positive for PDGFR. Percentage of areas positive for C1qa were normalized to percentage area positive for F4/80. Regions of interest were taken from three to four samples per group, with two to four regions of interests per animal. Percent area positive for expression were graphed for each group and statistical significance was determined by unpaired T test using GraphPad Prism (Prism10).

Evaluation of lung lesion size and number

H&E-stained sections of murine lungs were scanned using the Nikon Supercool Scan 5000 at 1X magnification. Evaluation of lung lesion number and size was blinded and performed on at least five sections per experimental group by three different readers. The number of lesions was graphed

for each group and statistical significance was determined by Ordinary one-way ANOVA using GraphPad Prism (Prism10).

Microcomputed tomography (CT imaging)

μCT imaging was performed similarly to methods previously described [38]. In brief, imaging was performed at indicated timepoints using Bruker SkyScan 1176 System with the following parameters: 60 kilovolt peaks (kVp) with a 1 mm aluminum filter, 168 μA, 158-ms exposure, 0.5° rotation step over 360°, and a reconstructed voxel size of 35-μm.

Quantitative Real-Time PCR (qRT-PCR)

Total RNA was extracted using the RNeasy Mini Kit (Qiagen). Purified total RNA samples were quantified at the spectrophotometer (NanoDrop ND-1000, NanoDrop Technologies). cDNA was synthesized using random hexamers and oligo-dT primers (QuantiTect Reverse Transcription Kit, Qiagen), in 2720 Thermal Cycler (Biorad). cDNA samples for quantitative Real-Time PCR were prepared using a mix of 1× Fast-SYBR Green PCR Master Mix (Applied Biosystems) and the primers listed in **Supplemental Table 2**. qRT-PCR was performed in technical and biological triplicates, in QuantStudio3 thermal cycler (Applied Biosystems). Ppia and beta-actin were used as housekeeping control. Data were analyzed through relative quantification with the –ΔΔCt method.

Western blotting

Tissues were homogenized and lysed with RIPA lysis buffer (Thermo Fisher Scientific) supplemented with protease inhibitors (Complete Protease Inhibitor Cocktail, Roche) and phosphatase inhibitors (PhosSTOP, Roche). Similarly, cells were lysed with RIPA lysis buffer (Thermo Fisher Scientific) supplemented with protease inhibitors (Complete Protease Inhibitor

Cocktail, Roche) and phosphatase inhibitors (PhosSTOP, Roche). Protein concentrations of whole-cell lysates were determined using Lowry assays (Bio-Rad). 20 µg of total protein were prepared in LDS sample buffer (Invitrogen), separated on denaturing Bis-Tris gel (Invitrogen), and transferred to nitrocellulose membranes (GE Healthcare). Membranes were blocked in 5% milk in 0.1% Tween 20 Tris-buffered saline (TBST) and subsequently incubated with primary antibodies against phospho-p44/42 MAPK (pErk1/2; Thr202/Tyr204), total ERK, RasG12D, and P53 (Cell Signaling Technology) in TBST overnight at 4°C, or with β Actin HRP-conjugated for 1 hour at room temperature. Secondary antibodies were purchased from Jackson ImmunoResearch. ECL-Plus substrate (Bio-Rad) and Bio-Rad ChemiDoc MP imager were used according to the manufacturer's recommendations.

Cell Lines

Primary mouse lung cancer cell line LC3-457, derived from the CCSP-rtTA; TetO-KRAS^{G12D}; Trp53$^{LSL-R172H}$ mouse model, was established starting from lung tissue of GEMM mice treated with doxycycline and AdCre. In LC3-457 cells oncogenic Kras expression can be induced or inactivated by addition of 1µg/ml of doxycycline hyclate (Sigma Aldrich) to medium or withdrawn by replacing with media excluding doxycycline. These cells were used at low passage, genotyped for the *Kras*, *Cre*, and *p53* transgenes, and tested negative for mycoplasma. NLF-2522 was isolated from normal lung tissue of control mice. Both cell lines were cultured in DMEM (Gibco) with 10% HI-FBS (Gibco) and 1% Pen/Strep (Gibco). The KPL86 primary mouse lung cancer cell line was generously provided by Dr. David DeNardo and has been previously described [20]. Briefly, the KPL86 cell line was generated from lung tissues of 9-month-old Kras$^{LSL-G12D}$;p53$^{flox/+}$ mice treated with ad-Cre recombinase. KPL86 cells were maintained in collagen-coated tissue culture dishes in DMEMF12 (Gibco) with 10% HI-FBS (Gibco) and 1% Pen/Strep (Gibco). The human

lung adenocarcinoma A-549 and A-427 cell line were obtained from ATCC (ATCC® CCL-185™ and CRL-1642™, respectively) and maintained in RPMI with 10% HI-FBS and 1% Pen/Strep (Gibco). Human Fibroblast CCL-210 cell line was kindly provided by Dr. Peters-Golden from the University of Michigan. This cell line was cultured in DMEM low Glucose (Gibco) with 10% HI-FBS (Gibco), 1X of GlutaMAX-I supplement (Gibco) and 1X of Antibiotic-Antimycotic (Gibco). All cells were cultured at 37°C with 5% CO2 and monthly mycoplasma testing was performed with the MycoAlert Mycoplasma Detection Kit (LT07-318, Lonza).

Conditioned media experiments

Conditioned media experiments with murine cells: To generate conditioned media from the LC3-457 murine cell line, 30% confluent LC3-457 was cultured in fresh media (DMEM with 1% HI-FBS and 1% Pen/Strep) containing doxy (ON), without doxy (OFF), or with doxy and 10-500 nM MRTX1133 (MRTX). Media were collected after 48 hours. Media were centrifuged at 300 × G for 10 minutes at 4°C and supernatant was collected to generate conditioned media (TCM: TCM ON, TCM OFF, TCM MRTX) for subsequent experiments. TCM were used to culture fibroblasts with a 3:1 ratio of TCM to normal DMEM with 1% HI-FBS for 24 hours. Along with TCM, aliquots of TCM or regular DMEM conditioned by fibroblasts (ON CAF CM, OFF CAF CM, MRTX CAF CM, and DMEM) were collected for multiplex ELISA Luminex analysis (see below).

Conditioned media experiments with human cell lines: To generate conditioned media, fresh media with 100 nM MRTX1133 or equimolar concentration of DMSO ($Kras^{G12D}$ ON) was replaced and harvested after two days. TCM was harvested and processed as described for murine TCM then used to condition CCL-210 fibroblasts for 24 hours.

Bone marrow isolation and macrophage polarization: TCM or CAF CM were used for the macrophage polarization assay. For macrophage polarization, bone marrow tissue was isolated from WT mice femurs and tibia, carefully flushing out the marrow until the bone was white, which indicates that all marrow has been removed. Cells were centrifuged at 1,500 rpm for 7 min at 4 °C and then pellet was incubated with 1 ml red blood cell lysis buffer. Once isolated, 2×10^6 BMDM cells were cultured directly with CM for 6 days. Fresh CM were added on the third day. This process allowed the differentiation and polarization of BMDM cells to tumor associated macrophages (TAMs). BMDMs from the ON + CXCRi group were treated with 10 nM CXCR2 inhibitor SB225002 (cat number: S7651; Selleckchem). After 6 days TAMs were harvested and lysed to extract total RNA.

Multiplex ELISA (Luminex)

Mouse: 200 μL of conditioned media for each sample were collected and centrifuged before supernatants were stored at -80° C. Multiplex ELISA (Luminex) was performed by the Michigan Diabetes Research Center (MDRC) Chemistry Laboratory. For murine generated TCM and FCM, the MILLIPLEX® Mouse Cytokine/Chemokine Magnetic Bead kit (MCYTMAG-70K-PX32) was used for detecting the following analytes in TCM and FCM: Eotaxin, G-CSF, GM-CSF, IFNγ, IL-1α, IL-1β, IL-2, IL-3, IL-4, IL-5, IL-6, IL-7, IL-9, IL-10, IL-12 (p40), IL-12 (p70), IL-13, IL-15, IL-17, IP-10, KC, LIF, LIX, MCP-1, M-CSF, MIG, MIP-1α, MIP-1β, MIP-2, RANTES, TNFα, and VEGF. Simultaneous quantification of analytes was performed on the Luminex ® 200™ instrument.

Human: 200 μL of conditioned media for each sample were collected and centrifuged before supernatants were stored at -80° C. Multiplex ELISA was performed by the Michigan Diabetes

Research Center (MDRC) Chemistry Laboratory. MILLIPLEX® Human Cytokine/Chemokine Magnetic Bead kit (HCYTA-60K-PX48) was used for detecting the following analytes in TCM and CAF CM: sCD40L, EGF, FGF-2, Flt3, CX3CL1, Eotaxin, G-CSF, GM-CSF, GROα, IFNα2, IFNγ, IL-1α, IL-1β, IL-1RA, IL-2, IL-3, IL-4, IL-5, IL-6, IL-7, IL-9, IL-10, IL-12 (p40), IL-12 (p70), IL-13, IL-15, IL-17A, IL-17E, IL-17E, IL-17F, IL-18, IL-18, IL-22, IL-27, IP-10, KC, LIF, LIX, MCP-1, MCP-3, MDC, M-CSF, MIG, MIP-1α, MIP-1β, MIP-2, PDGF-AB/BB, RANTES, TGFα, TNFα, and VEGF-A. Simultaneous quantification of analytes was performed on the Luminex ® 200™ instrument.

Acknowledgements and Funding

This work was supported by the National Cancer Institute (NCI) of the National Institutes of Health (NIH) Grant 1R21CA286372 (to S. Galban and M. Pasca di Magliano), the University of Michigan Rogel Cancer Center First and Goal Award (to S. Galban), the National Institute of Diabetes and Digestive and Kidney Diseases of NIH Grant P30DK020572, which funds the Michigan Diabetes Research Center at the University of Michigan; the University of Michigan Cancer Biology T32 Training Grant T32-CA009676 (to E. Lasse-Opsahl); the National Science Foundation Graduate Research Fellowship Program (to R. Baliira); the University of Michigan Rackham Merit Fellowship (to R. Baliira); NCI/NIH Grant F31-CA265085 (to K. Donahue); and NCI/NIH Grants R01 CA260752, R01 CA271510, U01 CA224145, U01 CA274154, and U54 CA274371, which fund the M. Pasca di Magliano Laboratory. We would like to thank Dr. David DeNardo (Washington University in St. Louis) for generously providing the KPL86 primary mouse lung cancer cell line. We would like to thank members of the Galban lab and Pasca lab, especially Lily Rober and Alanna Devorkin for their assistance with some experiments. We would also like to acknowledge the scRNA seq core, histology core and Luminex core at the University of Michigan for their support.

References

1. Maroni, G., et al., *Identification of a targetable KRAS-mutant epithelial population in non-small cell lung cancer.* Commun Biol, 2021. **4**(1): p. 370.
2. Yu, H.A., et al., *Prognostic impact of KRAS mutation subtypes in 677 patients with metastatic lung adenocarcinomas.* J Thorac Oncol, 2015. **10**(3): p. 431-7.
3. Society, A.C., *Cancer Facts & Figures 2021.* Cancer Facts & Figures is an annual publication of the American Cancer Society, Atlanta, Georgia, 2021.
4. Zhao, W., et al., *Impact of Smoking History on Response to Immunotherapy in Non-Small-Cell Lung Cancer: A Systematic Review and Meta-Analysis.* Front Oncol, 2021. **11**: p. 703143.
5. Di Federico, A., et al., *Resistance to KRAS G12C Inhibition in Non-small Cell Lung Cancer.* Curr Oncol Rep, 2023. **25**(9): p. 1017-1029.
6. Balachandran, V.P., et al., *Identification of unique neoantigen qualities in long-term survivors of pancreatic cancer.* Nature, 2017. **551**(7681): p. 512-516.
7. Tsai, Y.S., et al., *Rapid idiosyncratic mechanisms of clinical resistance to KRAS G12C inhibition.* J Clin Invest, 2022. **132**(4).
8. DuPage, M., A.L. Dooley, and T. Jacks, *Conditional mouse lung cancer models using adenoviral or lentiviral delivery of Cre recombinase.* Nat Protoc, 2009. **4**(7): p. 1064-72.
9. Fisher, G.H., et al., *Induction and apoptotic regression of lung adenocarcinomas by regulation of a K-Ras transgene in the presence and absence of tumor suppressor genes.* Genes Dev, 2001. **15**(24): p. 3249-62.
10. Xu, X., et al., *Evidence for type II cells as cells of origin of K-Ras-induced distal lung adenocarcinoma.* Proc Natl Acad Sci U S A, 2012. **109**(13): p. 4910-5.
11. Ferone, G., et al., *Cells of origin of lung cancers: lessons from mouse studies.* Genes Dev, 2020. **34**(15-16): p. 1017-1032.
12. Jackson, E.L., et al., *Analysis of lung tumor initiation and progression using conditional expression of oncogenic K-ras.* Genes Dev, 2001. **15**(24): p. 3243-8.
13. Hingorani, S.R., et al., *Trp53R172H and KrasG12D cooperate to promote chromosomal instability and widely metastatic pancreatic ductal adenocarcinoma in mice.* Cancer Cell, 2005. **7**(5): p. 469-83.
14. Steele, N., et al., *Abstract 3855: Oncogenic Kras-mediated regulation of the tumor microenvironment in lung cancer.* Cancer Research, 2020. **80**(16_Supplement): p. 3855-3855.
15. Jackson, E.L., et al., *The differential effects of mutant p53 alleles on advanced murine lung cancer.* Cancer Res, 2005. **65**(22): p. 10280-8.
16. Kim, N., et al., *Single-cell RNA sequencing demonstrates the molecular and cellular reprogramming of metastatic lung adenocarcinoma.* Nat Commun, 2020. **11**(1): p. 2285.
17. Bischoff, P., et al., *Single-cell RNA sequencing reveals distinct tumor microenvironmental patterns in lung adenocarcinoma.* Oncogene, 2021. **40**(50): p. 6748-6758.
18. Velez-Delgado, A., et al., *Extrinsic KRAS Signaling Shapes the Pancreatic Microenvironment Through Fibroblast Reprogramming.* Cell Mol Gastroenterol Hepatol, 2022.
19. Kemp, S.B., et al., *Pancreatic cancer is marked by complement-high blood monocytes and tumor-associated macrophages.* Life Sci Alliance, 2021. **4**(6).
20. Herzog, B.H., et al., *Tumor-associated fibrosis impairs immune surveillance and response to immune checkpoint blockade in non–small cell lung cancer.* Science Translational Medicine. **15**(699): p. eadh8005.
21. Goenka, S. and M.H. Kaplan, *Transcriptional regulation by STAT6.* Immunol Res, 2011. **50**(1): p. 87-96.

22. Roszer, T., *Understanding the Mysterious M2 Macrophage through Activation Markers and Effector Mechanisms.* Mediators Inflamm, 2015. **2015**: p. 816460.
23. Stuart, T., et al., *Comprehensive Integration of Single-Cell Data.* Cell, 2019. **177**(7): p. 1888-1902.e21.
24. Kemp, S.B., et al., *Apolipoprotein E Promotes Immune Suppression in Pancreatic Cancer through NF-kappaB-Mediated Production of CXCL1.* Cancer Res, 2021. **81**(16): p. 4305-4318.
25. Biankin, A.V., et al., *Pancreatic cancer genomes reveal aberrations in axon guidance pathway genes.* Nature, 2012. **491**(7424): p. 399-405.
26. Hsu, W.H., et al., *Oncogenic KRAS Drives Lipofibrogenesis to Promote Angiogenesis and Colon Cancer Progression.* Cancer Discov, 2023. **13**(12): p. 2652-2673.
27. *FDA Approves First KRAS Inhibitor: Sotorasib.* Cancer Discov, 2021. **11**(8): p. OF4.
28. Hong, D.S., et al., *KRAS(G12C) Inhibition with Sotorasib in Advanced Solid Tumors.* N Engl J Med, 2020. **383**(13): p. 1207-1217.
29. Lanman, B.A., et al., *Discovery of a Covalent Inhibitor of KRAS(G12C) (AMG 510) for the Treatment of Solid Tumors.* J Med Chem, 2020. **63**(1): p. 52-65.
30. Wang, X., et al., *Identification of MRTX1133, a Noncovalent, Potent, and Selective KRAS(G12D) Inhibitor.* J Med Chem, 2022. **65**(4): p. 3123-3133.
31. Chen, H. and J. Zhao, *KRAS oncogene may be another target conquered in non-small cell lung cancer (NSCLC).* Thorac Cancer, 2020. **11**(12): p. 3425-3435.
32. Olive, K.P., et al., *Mutant p53 gain of function in two mouse models of Li-Fraumeni syndrome.* Cell, 2004. **119**(6): p. 847-60.
33. Ramilowski, J.A., et al., *A draft network of ligand-receptor-mediated multicellular signalling in human.* Nat Commun, 2015. **6**: p. 7866.
34. Steele, N.G., et al., *Multimodal Mapping of the Tumor and Peripheral Blood Immune Landscape in Human Pancreatic Cancer.* Nat Cancer, 2020. **1**(11): p. 1097-1112.
35. Shannon, P., et al., *Cytoscape: a software environment for integrated models of biomolecular interaction networks.* Genome Res, 2003. **13**(11): p. 2498-504.
36. Carpenter, E.S., et al., *Analysis of Donor Pancreata Defines the Transcriptomic Signature and Microenvironment of Early Neoplastic Lesions.* Cancer Discov, 2023. **13**(6): p. 1324-1345.
37. Shamonin, D.P., et al., *Fast parallel image registration on CPU and GPU for diagnostic classification of Alzheimer's disease.* Front Neuroinform, 2013. **7**: p. 50.
38. Bowman, B.M., et al., *Phosphorylation of FADD by the kinase CK1alpha promotes KRASG12D-induced lung cancer.* Sci Signal, 2015. **8**(361): p. ra9.